AIMS Energy, 12(6): 1096–1112.
DOI: 10.3934/energy.2024052
Received: 29 July 2024
Revised: 11 October 2024
Accepted: 18 October 2024
Published: 28 October 2024

http://www.aimspress.com/journal/energy

Research article

Recognition of partial discharge in GIS based on image feature fusion

Ziqiang Xu, Honghua Xu*, Chao Yuan, Shoulong Chen and Yini Chen

Nanjing Power Supply Company, State Grid Jiangsu Electric Power Co., Ltd, Nanjing 210000, China

* **Correspondence:** Email: alex7776@126.com; Tel: +8618955452579.

Abstract: Partial discharge (PD) is a significant electrical fault in gas-insulated switchgear (GIS), with various types posing different risks to insulation. Accurate identification of PD types is essential for enhancing GIS management and ensuring the reliability of electrical grids. This study proposes a novel approach for PD identification in GIS integrating completed local binary pattern (CLBP) feature extraction, feature engineering, and an optimized support vector machine (SVM). PD faults were simulated in GIS and phase-resolved pulse sequence (PRPS) data for four different forms of PD were gathered. CLBP was used to extract image features, and then the support vector machine recursive feature elimination (SVM-RFE) algorithm was used to evaluate feature importance. Then, linear discriminant analysis (LDA) was used to fuse the selected features and reduce redundancy. The fused features were classified using a bald eagle search algorithm combined with differential evolution (IBES)-optimized SVM, achieving a recognition accuracy of 99.38%. The results indicate that the proposed method effectively distinguishes between different PD PRPS patterns in GIS.

Keywords: phase-resolved pulse sequence; gas-insulated switchgear; support vector machine; intelligent optimization algorithm; local binary patterns

1. Introduction

Gas-insulated switchgear (GIS) has the advantages of large capacity, high reliability, and environmental friendliness, making it widely used in modern power systems [1]. During manufacturing, transportation, assembly, and operation of GIS, insulation defects may arise due to human factors and other variables, which can worsen under high voltage conditions and lead to partial discharge (PD) [2,3]. Detecting partial discharge enables timely identification of insulation defects within GIS equipment, preventing serious equipment failures [4].

The ultra-high frequency (UHF) method uses UHF sensors to detect electromagnetic waves emitted during the PD processes for efficient detection [5]. The UHF method characterizes high sensitivity and strong resistance to electromagnetic interference. However, the ultra-high frequency signals are complex and require a combination of signal processing and pattern recognition techniques to enhance the recognition accuracy of partial discharge categories [6].

The commonly used recognition models currently include machine learning models such as support vector machines [7,8], extreme learning machines [9,10], and deep learning models such as convolutional neural networks (CNN) [11–13]. In [14] the phase-resolved pulse sequence (PRPS) image of partial discharge pulse signals was enhanced using contrast-limited adaptive histogram equalization. Then, uniform local binary mode was used to extract features from the enhanced PRPS image. Finally, it is fed into the Adaboost classifier, improving recognition accuracy and training efficiency. Considering single PD data and noisy PD data, authors in [15] used the SURF algorithm to extract PRPS grayscale image features combined with K-means to extract visual word frequency features and finally input the extracted image features into the bacterial foraging algorithm-improved support vector machine (BFO-SVM) model to achieve partial discharge type recognition. In [16], the authors proposed a method for GIS partial discharge identification combining Zernike and improved SVM. By extracting PRPS image features using Zernike moment and employing an optimized SVM, an identification accuracy of 91.23% was achieved. In [17], authors introduced a UHF data preprocessing method based on projection, using PRPS images, partial discharge pattern detector (PRPD) images, and projection images as input data for CNN, achieving good identification results. In [18], a GIS partial discharge identification method was proposed, based on a histogram of oriented gradient (HOG) image features and a naive Bayes classifier, which has a relatively simple preprocessing and training process. In [19], a GIS partial discharge identification method based on deep convolutional neural networks was introduced, which improved model recognition performance by constructing complex datasets. In [20], authors proposed a novel hybrid meta-learning method for insulation defect diagnosis in small sample GIS, which can achieve good recognition performance even under small sample conditions. In [21], a metric-based meta-learning approach was proposed, which significantly improves over traditional methods under a few sample conditions.

A significant issue in GIS partial discharge model training is the lack of training data. SVM is highly applicable in small sample scenarios. However, the recognition accuracy of SVM models is influenced by the parameters c and g. Manual parameter tuning is inefficient, and using intelligent optimization algorithms to search for parameters can effectively improve model recognition accuracy.

To reduce the cost of model training, it is necessary to extract features from PRPS images. However, extracted features may have a weak correlation with the category of partial discharge, which may affect the recognition accuracy. Therefore, it is necessary to evaluate the importance of features and select the most important ones. In addition, to reduce redundancy in feature data, the selected features should be fused before inputting into the recognition module.

The main contributions of this paper are as follows:

(1) To address the issue of redundancy in image features, this paper proposes a feature processing method combining support vector machine-recursive feature elimination (SVM-RFE) with linear discriminant analysis (LDA). This method effectively eliminates redundant features, significantly reducing the complexity of the model and lowering computational cost.

(2) Proposes an improved bald eagle search algorithm combined with differential evolution (IBES), enhancing the search process's performance. The IBES-SVM model demonstrates superior recognition performance compared to other benchmark methods.

(3) Through partial discharge simulation experiments, PRPS spectrograms for various types of

GIS partial discharges were collected. The experimental results show that the proposed method can effectively identify different types of partial discharges, providing a novel approach for GIS partial discharge diagnosis.

2. Methods

2.1. Feature extraction of PRPS images based on CLBP

The CLBP [22] extracts image features by comparing the values of the center pixel and domain pixels after image segmentation. If the domain value is larger than the center point, it is 1; otherwise, it is 0. The three operators CLBP-C, CLBP-S, and CLBP-M reflect the grayscale value, sign information, and amplitude information of the central pixel in the image. The expressions for these three operators are:

$$CLBP\_C_{P,R} = t(g_c, c_I), t(x,c) = \begin{cases} 1, & x \geq c \\ 0, & x < c \end{cases} \tag{1}$$

$$CLBP\_S_{P,R} = \sum_{P=0}^{P-1} s\left(s_p\right) 2^p, s(x) = \begin{cases} 1, & x \geq c \\ 0, & x < c \end{cases} \tag{2}$$

$$CLBP\_M_{P,R} = \sum_{P=0}^{P-1} t\left(m_p, c\right) 2^p, t(x,c) = \begin{cases} 1, & x \geq c \\ 0, & x < c \end{cases} \tag{3}$$

In the formulas, g_c represents the center pixel of a certain point, c_I represents the average grayscale value of image pixels, and c is the adaptive threshold represented by the mean of m_p in the entire image. d_p is a local difference vector between a central pixel and P neighboring values, where s_p and m_p are the sign and amplitude values of d_p, respectively.

2.2. PRPS image feature selection based on SVM-RFE

The high dimensionality of image features leads to feature redundancy, so it is necessary to rank the importance of these features and select the most important ones to improve the accuracy and speed of GIS partial discharge recognition models.

SVM-RFE [23,24] is a feature selection method combining SVM with RFE, where the weight of each feature reflects its impact on the classification results. SVM-RFE ranks features based on their weights and iteratively eliminates less important features while retaining important ones. The detailed steps for selecting features from GIS partial discharge images using SVM-RFE are as follows:

Step 1: Input feature data $F = \left[f_1, f_2, \ldots, f_n\right]^T$ and label data $L = \left[l_1, l_2, \ldots, l_n\right]^T$.

Step 2: Initialize feature importance $W = [w_1, w_2, \ldots, w_n]$ and reordered feature importance $W^* = \left[w_1^*, w_2^*, \ldots w_N^*\right]$.

Step 3: Train the input data using an SVM classifier to obtain the weights of the features.

Step 4: Calculate the cost function of the features:

$$f(x) = \frac{1}{2} F^T U(x) - \frac{1}{2} F^T U(-x) \tag{4}$$

In the equations, U is a matrix with elements $l_{ij}K(x_i, x_j)$, $U(-x)$ is the matrix after eliminating x features, and K is the kernel function representing the correlation between x_i and x_j.

Step 5: Reorder the features based on the weights $W^* = \left[w_1^*, w_2^*, \ldots w_N^*\right]$.

Step 6: Select the final subset of features $W^* = \left[w_1^*, w_2^*, \ldots w_n^*\right]$ based on the SVM classification accuracy.

2.3. Image feature fusion based on LDA

To further reduce the dimensionality of features, we use LDA [25] to fuse the selected features. The specific steps of the LDA dimensionality reduction method are as follows:

(1) Calculate the n-dimensional mean vectors for each class from the dataset.

(2) Compute the scatter matrices.

(3) Calculate the eigenvectors $(e_1, e_2, \ldots, e_n)$ and their corresponding eigenvalues $(\lambda_1, \lambda_2, \ldots, \lambda_n)$ of the scatter matrices.

(4) Arrange the feature vectors in descending order based on their eigenvalues, and select the top k feature vectors with the largest eigenvalues, forming a d × k dimensional matrix M.

(5) Map the samples to different subspaces using matrix M and obtain the LDA-reduced feature vector matrix Z through matrix multiplication, where Z = X × M and X is the given data matrix.

2.4. Classifier based on IBES-SVM

The inspiration for the BES optimization algorithm [26] comes from the hunting behavior of bald eagles. The search parameter process includes three stages: defining the search space, searching for prey, and capturing prey. To enhance the robustness and global search capability of the BES, this study introduces a differential evolution strategy during the iterative process. The specific steps for optimizing the IBES algorithm are as follows:

(1) Determine the search scope. The bald eagle selects the search area, and at this stage, the bald eagle updates according to the following formula:

$$P_{i,new} = P_{best} + \alpha * \delta(P_{mean} - P_i) \quad (5)$$

In the formula, $P_{i,new}$ represents the new search position generated for the i-th time, P_{best} is the currently determined best search position, P_{mean} is the average distribution position of the previous i-1 searches, α is the control gain $\alpha \in [1.5, 2]$, and δ is a random number $\delta \in [-1, 1]$.

Step 2: Search for prey. The bald eagle searches for prey in the search space, and the formula for updating the bald eagle's position is as follows:

$$P_{i,new} = P_i + y_i * (P_i - P_{i+1}) + x_i * (P_i - P_{mean}) \quad (6)$$

In the formula, $x(i)$, $y(i)$ are the position of the bald eagle in polar coordinates after the *i*-th update.

Step 3: Capture prey. During this stage, the bald eagle, who is in the optimal position, and other individuals in the population simultaneously attack the prey. The changes in the bald eagle's position during this process are as follows:

$$P_{i,new} = rand * P_{best} + y1(i) * (P_i - c2 * P_{best}) + x1(i) * (P_i - c1 * P_{mean}) \quad (7)$$

In the equation, $x1_i$ and $y1_i$ are the polar coordinates of the bald eagle at this stage; *rand* is random numbers between (0,1); $c1$ and $c2$ are the optimal positions for bald eagles to move toward, with the intensity of motion at the center position taken as [1,2].

Step 4: Differential evolution mainly includes three processes: mutation, crossover, and selection. In this article, the specific formula for differential evolution is as follows:

$$\begin{cases} selection: \ U_{i,j} = \begin{cases} \hat{V}_{i,j}, \text{ if } f(\hat{V}_{i,j}) < f(P_{best,j}) \\ P_{best,j}, \text{ else} \end{cases} \\ mutation: \ V_{i,j} = P_{best,j} + F(P_{n,j} - P_{m,j}) \\ rossover: \ \hat{V}_{i,j} = \begin{cases} V_{i,j}, \text{ rand}(0,1) \le \text{CR or } j=\text{rand}(1,D) \\ P_{best,j}, \text{ else} \end{cases} \end{cases} \quad (8)$$

In the formula, $V_{i,j}$ is the mutated individual, $P_{best,j}$ is the j-th dimension of the optimal individual, F is the scaling factor, CR is the crossover probability, and f is the fitness function. Differential evolution selects individuals with low fitness after cross-mutation to replace the optimal solution, bringing the algorithm closer to the global optimal solution.

2.5. GIS partial discharge diagnosis method based on image feature fusion and IBES-SVM

This section presents a GIS partial discharge recognition method based on image feature fusion integrated with IBES-SVM. The identification process is illustrated in Figure 1.

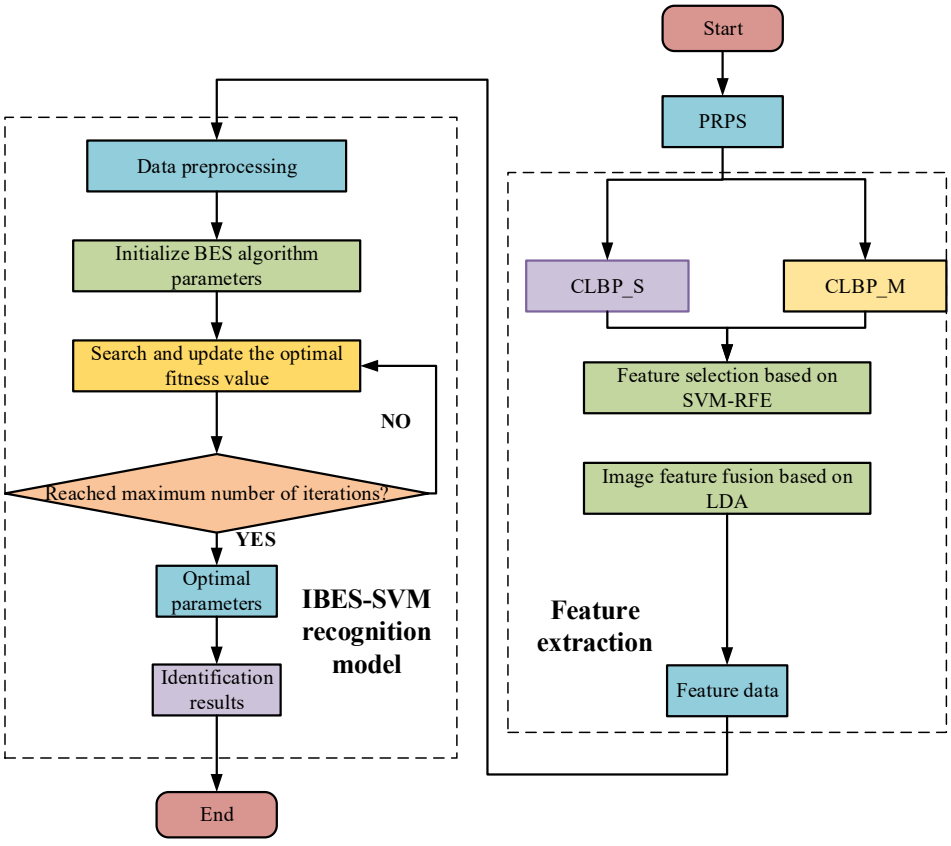

Figure 1. Algorithm flowchart.

(1) Extract features from PRPS images using CLBP_M and CLBP_S.

(2) Employ SVM-RFE with threshold selection to identify the ten most significant features from CLBP_S and CLBP_M.

(3) Apply the LDA algorithm to fuse the image features and eliminate redundant data.

(4) Normalize and randomly partition it into training and testing sets with a 3:2 ratio.

(5) Initialize the IBES-SVM model parameters and train the model using the training set.

(6) Input the test set data into the trained model, then output the recognition results.

3. GIS partial discharge experiment and map collection

To demonstrate the superiority of the proposed method in diagnosing GIS PD, four typical insulation defects were simulated on the GIS testing platform in the laboratory, and corresponding PD signals were collected. A UHF sensor detects the signals and converts them into data through an oscilloscope. Faults were simulated in the XD5936 GIS partial discharge simulation device, as shown in Figure 2.

Figure 2. GIS experimental device.

Four types of PD models—needle, surface, suspension, and gap—were sequentially placed in the chamber. An ultra-high frequency sensor, connected to an oscilloscope, was positioned in the external slot of the chamber and applied voltage to the GIS. As the voltage increased, the local fault models began to discharge, enabling the collection of UHF signals. For each fault type, 100 PRPS images were collected. Figure 3 presents the measured PRPS spectra, demonstrating significant differences in the peak values of the four PD signals across the quadrants.

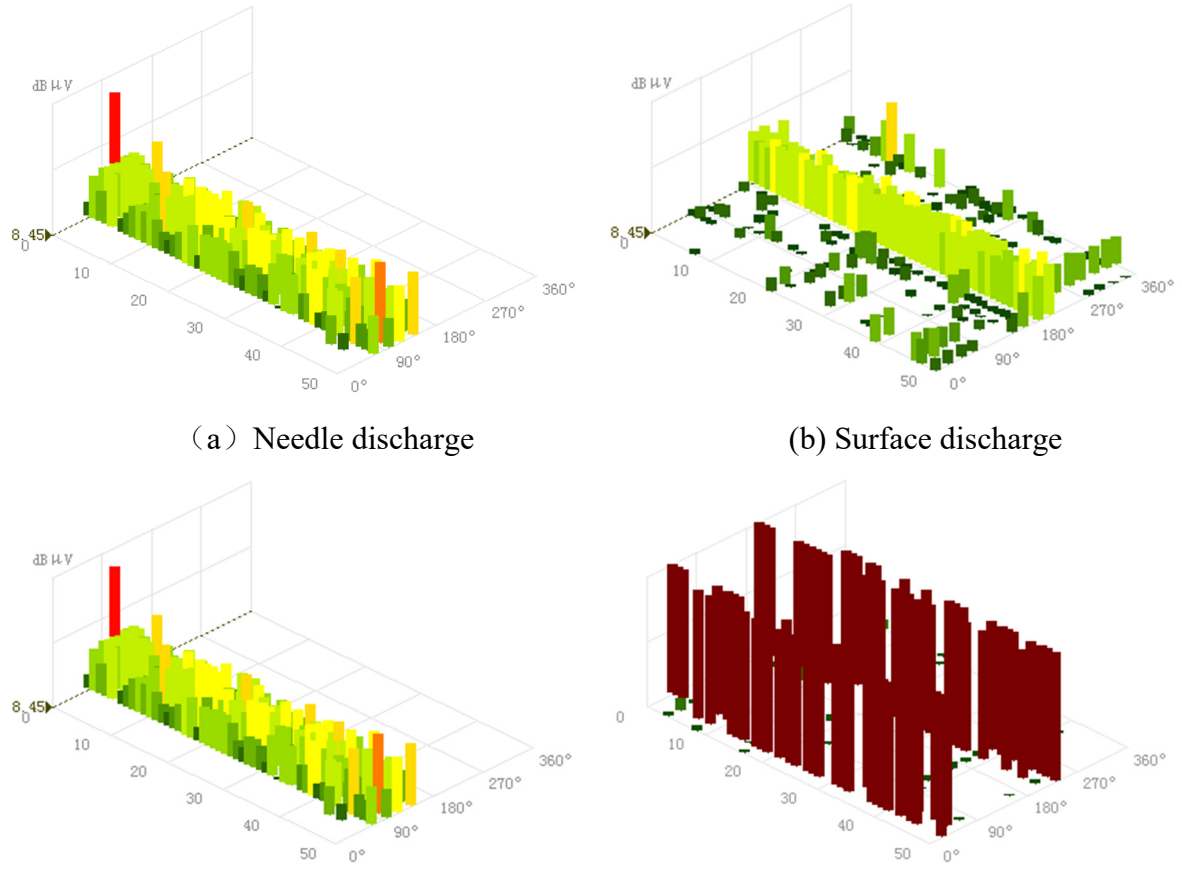

（a）Needle discharge (b) Surface discharge

(c) Gap discharge (d) Suspension discharge

Figure 3. Four types of partial discharge signals.

4. Experiment and analysis

4.1. Feature selection based on SVM-RFE

To accurately classify different types of partial discharges in various GIS systems, extracting features from PRPS images is essential. Considering the practical applicability of the method, this study used CLBP_S and CLBP_S operators to extract PRPS image features, both of which generate 59-dimensional features. The SVM-RFE algorithm was applied to select the most relevant features, effectively reducing the risk of gradient explosion. The feature importance ranking is presented in Figure 4.

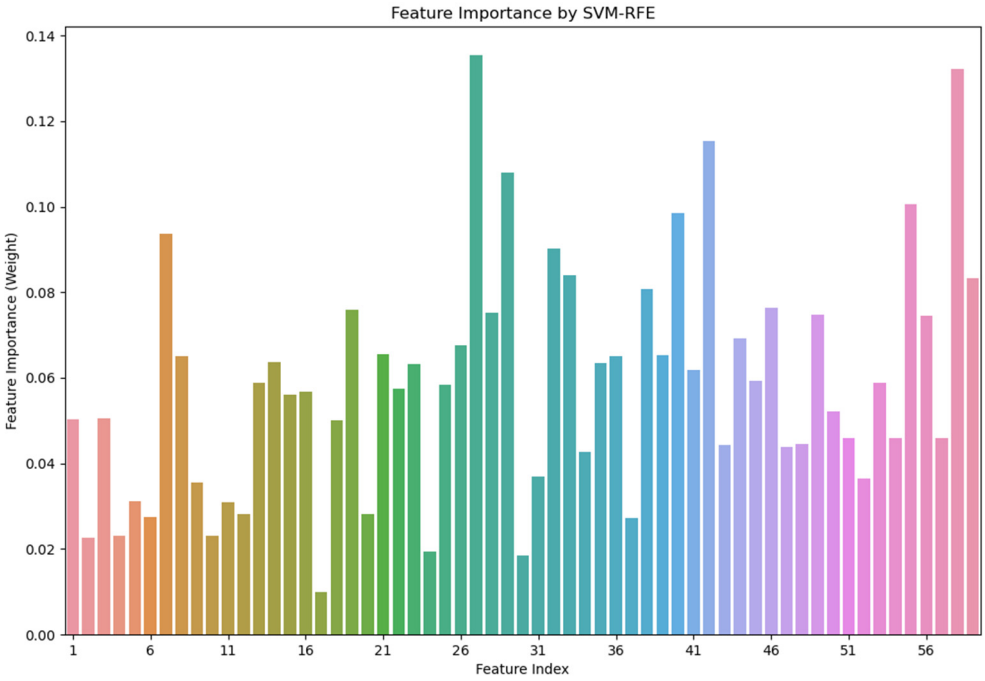

(a) CLBP_S feature extraction

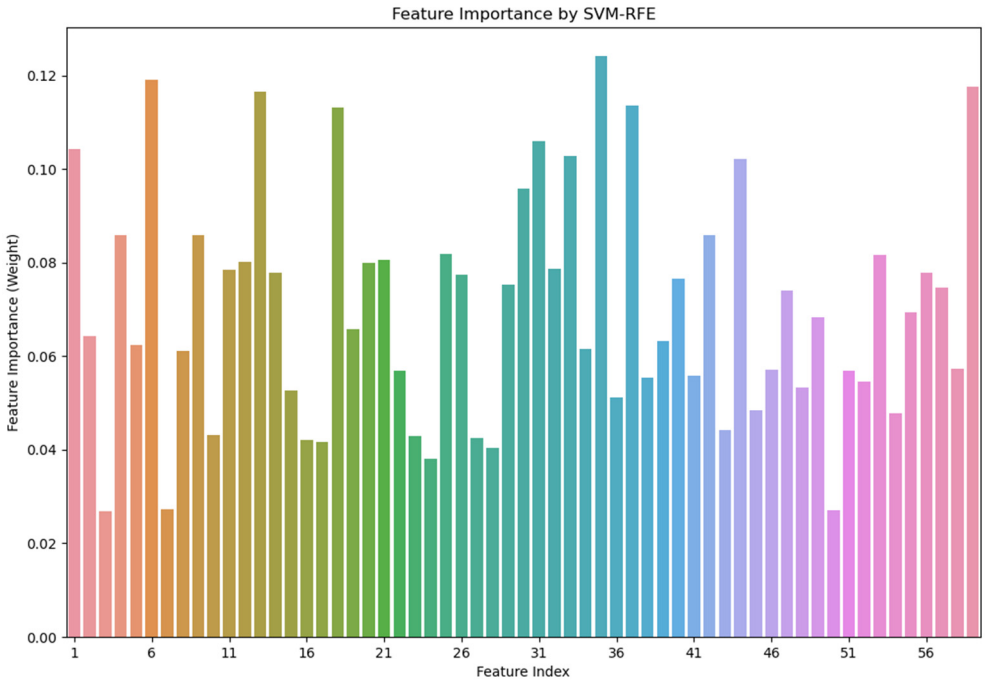

(b) CLBP_M feature extraction

Figure 4. SVM-RFE feature importance ranking.

Analysis of Figure 4 reveals significant differences in feature importance. For instance, the features extracted by the CLBP_S operator have weights of approximately 0.02 in the 3rd and 7th dimensions, while the weight in the 35th dimension exceeds 0.12. Including features with lower weights in the recognition process may decrease the accuracy of partial discharge type classification. Therefore, selecting relevant recognition features is essential.

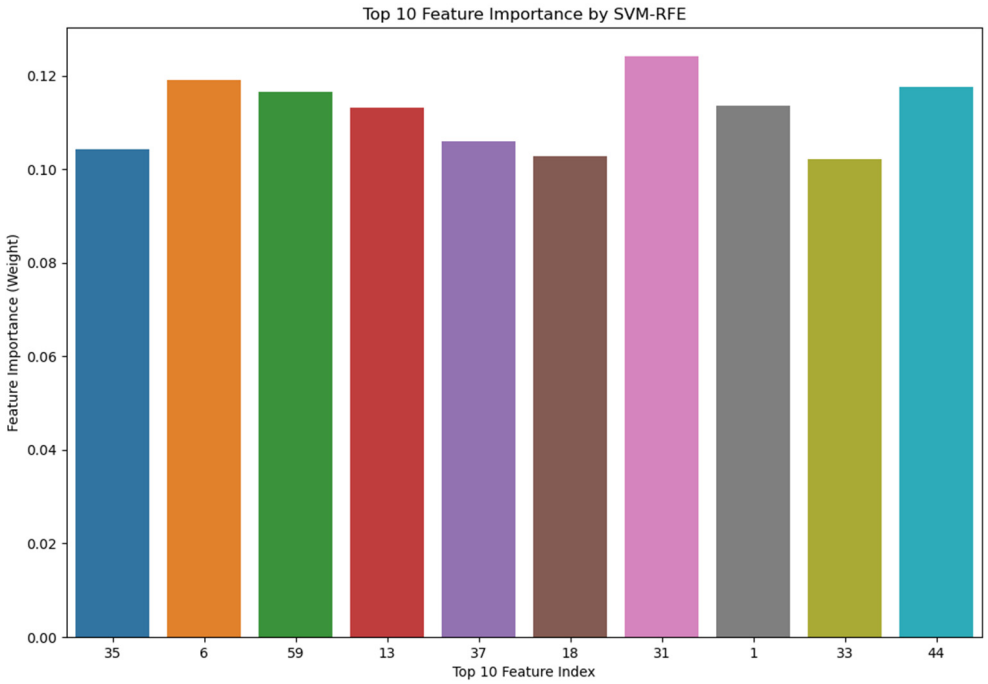

(a) Important features extracted using CLBP_S.

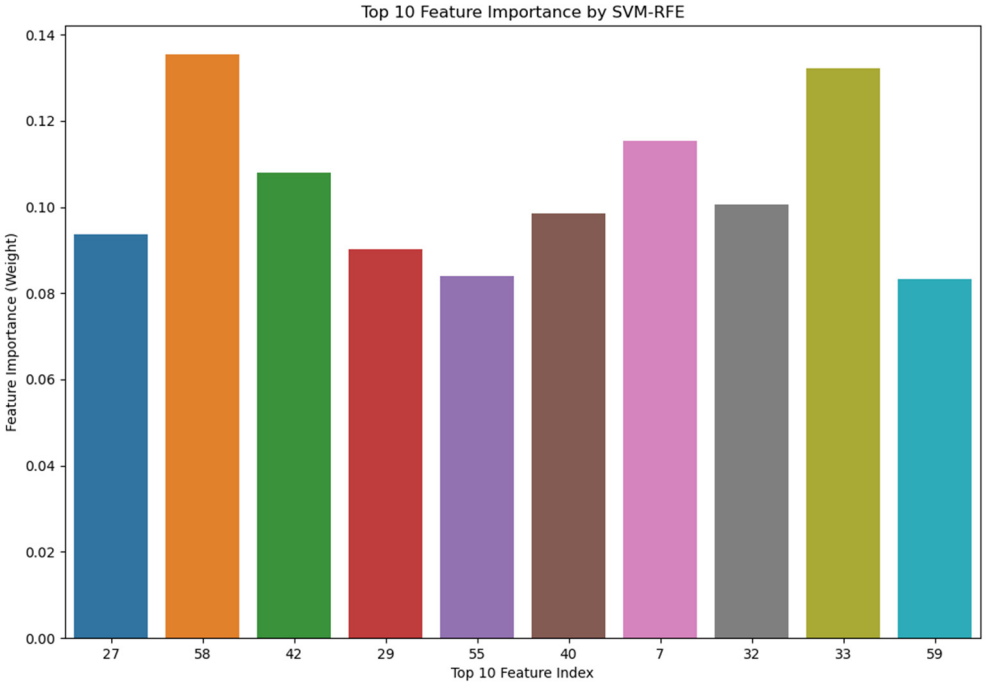

(b) Important features extracted using CLBP_M.

Figure 5. The top 10 most important features.

To effectively select significant features, we set the weight threshold at 0.08 and configured the target feature count for SVM-RFE to 10, as illustrated in Figure 5. The results reveal differences in the

dimensions and weights of the important features extracted by the two operators, suggesting that the features obtained from the two methods are complementary.

4.2. IBES algorithm

To verify the effectiveness of IBES, this study compared IBES, BES, artificial bee colony optimization (ABC), and dandelion optimization (DO) algorithms. The four test functions are shown in Table 1, with all algorithm iterations set to 100 and population size set to 50. The test results are shown in Figure 6.

Table 1. Objective function.

Objective function	Range	Dim
$F_1(X)=\sum_{i=1}^{m}x_i^2$	[–100, 100]	30
$F_2(X)=\sum_{i=1}^{m-1}\left[100\left(x_{i+1}-x_i^2\right)^2+\left(x_i-1\right)^2\right]$	[–30, 30]	30
$F_3(X)=\frac{\pi}{m}\left\{100\sin\left(\pi y_1\right)+\sum_{i=1}^{m}\left(y_i-1\right)^2\left[1+10\sin^2\left(\pi y_{i+1}\right)\right]+\left(y_n-1\right)^2\right\}$ $+\sum_{i=1}^{m}u\left(x_i,10,100,4\right)$	[–50, 50]	30
$y_i=\frac{x_i+1}{4},u\left(x_i,a,k,m\right)=\begin{cases}k\left(x_i-a\right)^m,x_i>a\\0,-a<x_i<a\\k\left(-x_i-a\right)^m,x_i<-a\end{cases}$		
$F_4(X)=\sum_{i=1}^{4}c_i\exp\left(-\sum_{j=1}^{6}a_{ij}\left(x_j-p_{ij}\right)^2\right)\left[100\left(x_{i+1}-x_i^2\right)^2+\left(x_i-1\right)^2\right]$	[0, 1]	6

From Figure 6, BES demonstrates the best convergence, while IBES outperforms ABC in convergence. Additionally, the optimization ability of the IBES algorithm is the strongest among the methods compared. This indicates that, although the convergence of the IBES algorithm has decreased after introducing differential evolution, its optimization effectiveness has significantly improved, making it more suitable for partial discharge recognition.

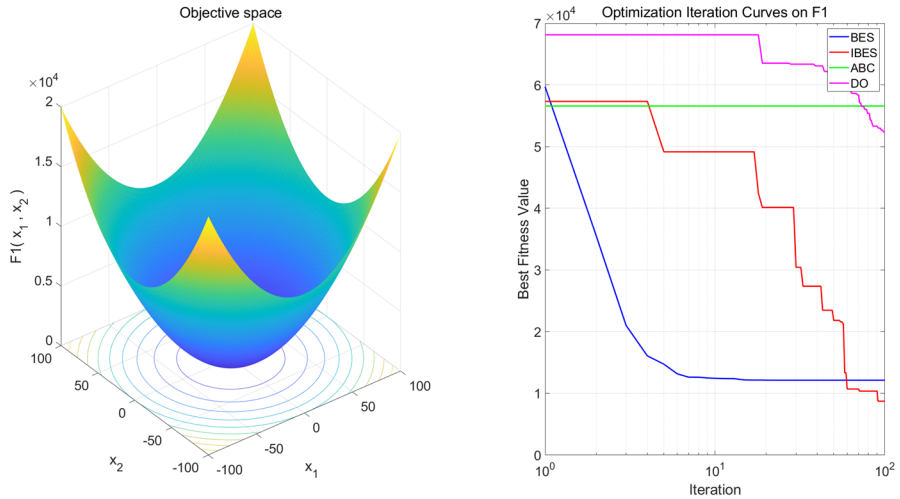

(a) F1

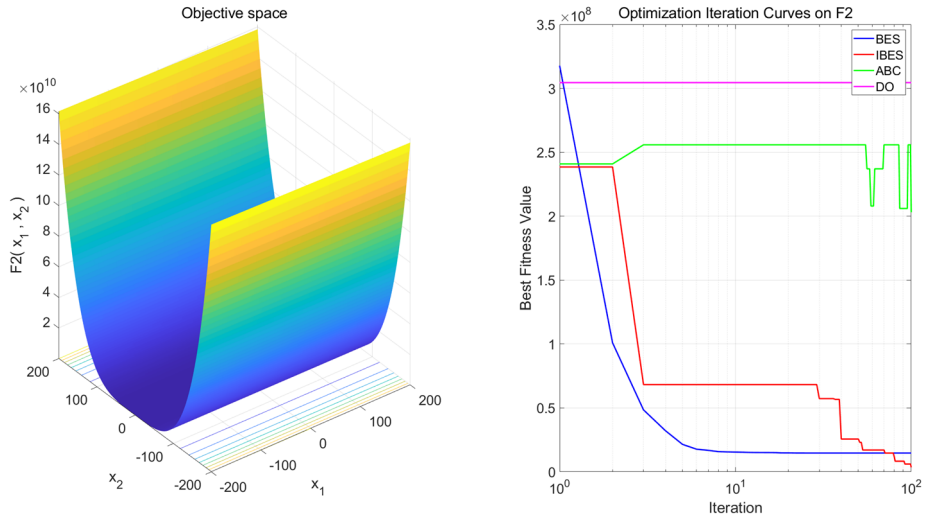

(b) F2

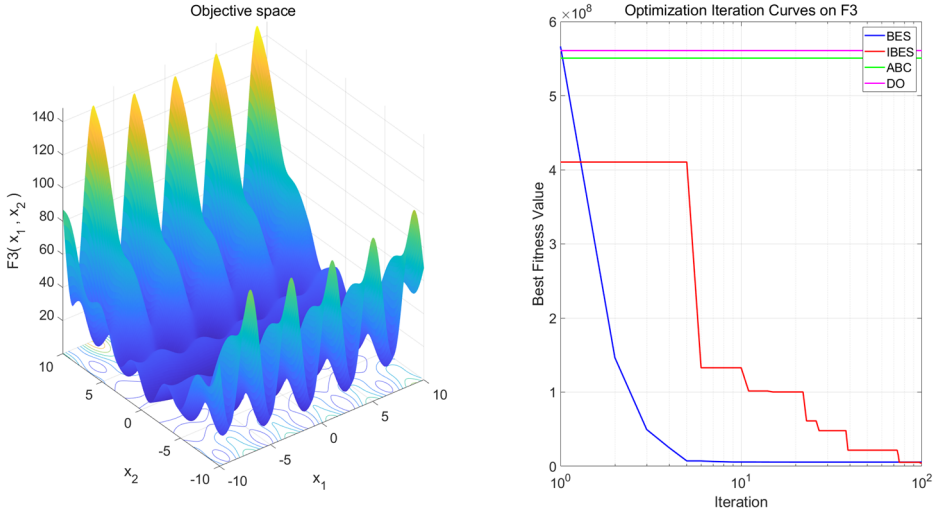

(c) F3

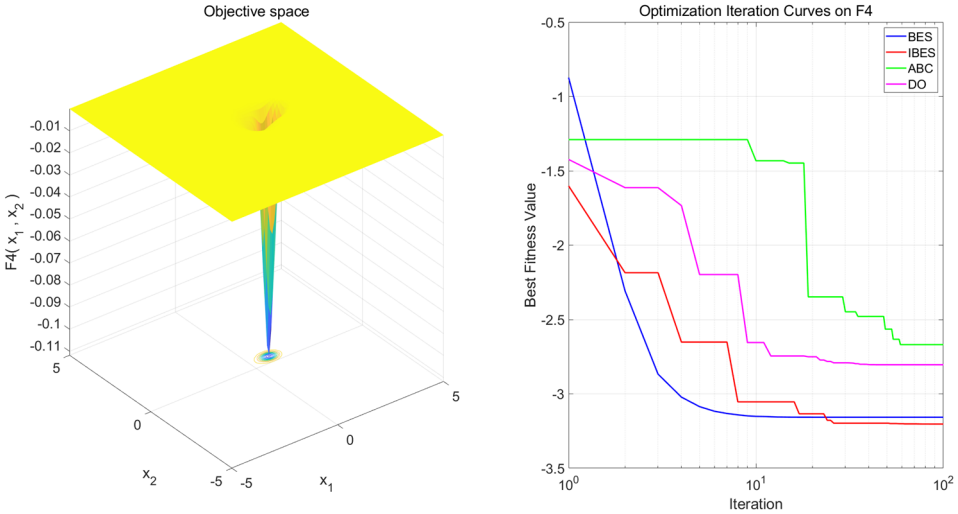

(d) F4

Figure 6. Results of objective functions.

4.3. Comparison of recognition performance across different classifiers

This study utilized the 10-dimensional CLBP_S features, 10-dimensional CLBP_M features, and 20-dimensional mixed features extracted in the previous section as inputs for the recognition models. The classifiers selected for evaluation include IBES-SVM, BES-SVM, artificial bee colony optimization SVM (ABC-SVM), and dandelion optimization SVM (DO-SVM).

The experimental results are shown in Table 2. The recognition model based on a single CLBP_S feature achieved accuracy higher than 80%, outperforming the model based on a single CLBP_M feature. When classifying using the three types of features, the IBES-SVM model demonstrated superior overall recognition performance. The recognition performance of the CLBP_S and CLBP_M mixed feature models was better than the other two single-feature models, with the recognition accuracy of all four classification models exceeding 90%.

Table 2. Three types of feature value feature recognition results.

Method	CLBP_S	CLBP_M	CLBP_S+CLBP_M
IBES-SVM	91.88%	81.88%	93.75%
BES-SVM	87.5%	78.75%	93.13%
ABC-SVM	84.38%	75%	90%
DO-SVM	85%	79.38%	92.5%

4.4. Comparison of different data fusion methods

To further enhance the model's accuracy in identifying discharge categories of GIS equipment, mixed features were subjected to data fusion using LDA, KPCA, and PCA. The visualization of the fusion results is presented in Figure 7. After data fusion, samples of the same category are more concentrated in feature space, while samples of different categories are more dispersed. Among the methods, LDA data fusion yielded the best results, whereas PCA fusion showed the poorest performance, with some overlap observed between needle discharge and gap discharge, as well as between surface discharge and gap discharge.

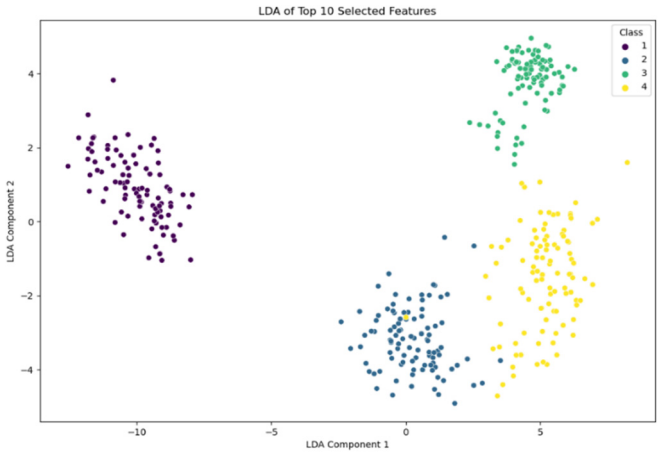

(a) LDA data fusion

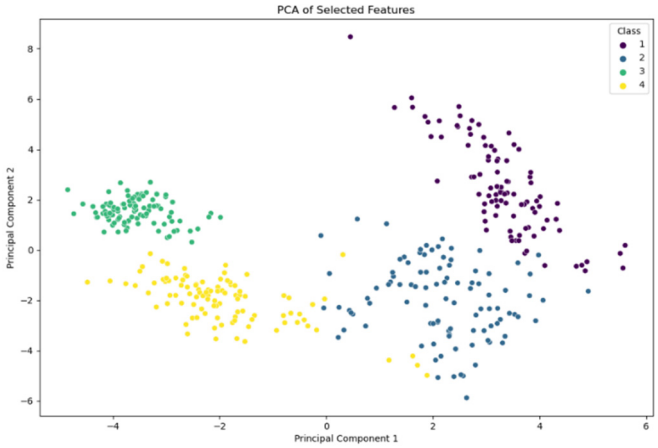

(b) PCA data fusion

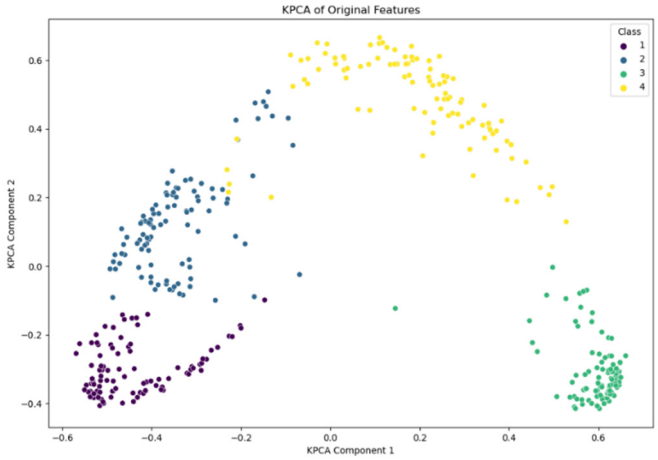

(c) KPCA data fusion

Figure 7. Visualization of results from three types of data fusion.

Some mixed samples of different categories remain in the feature space. In order to further improve the classification performance, we chose IBES-SVM, which had the best classification performance in the previous section, as the recognition model. The confusion matrix of the recognition results is shown in Figure 8, and the classification accuracy is shown in Table 3.

Table 3. Recognition results of different feature fusion models.

Method	Accuracy
LDA-IBES-SVM	99.38%
KPCA-IBES-SVM	98.13%
PCA-IBES-SVM	95.63%

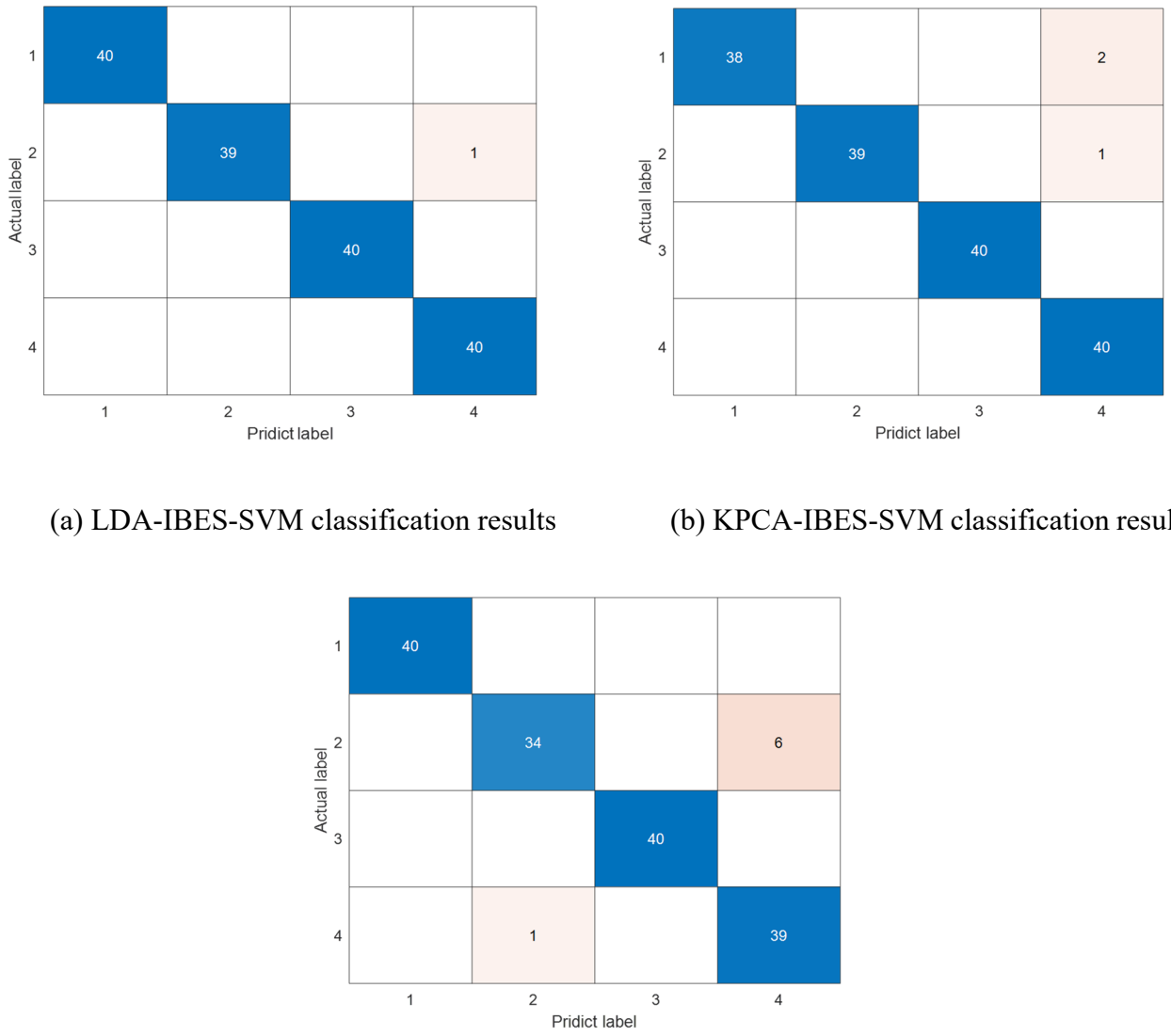

(a) LDA-IBES-SVM classification results

(b) KPCA-IBES-SVM classification results

(c) PCA-IBES-SVM classification results

Figure 8. Confusion matrix for different data fusion methods.

The LDA-IBES-SVM model misclassified one surface sample as gap discharge, while the KPCA-IBES-SVM model misidentified two needle samples as surface and another as gap. The PCA-IBES-SVM model classified six surface samples as gap and one gap sample as surface. The analysis indicates that recognition errors between surface and gap samples are frequent. The PRPS spectral image features of these two types are similar, and the image features of the suspended samples do not show significant differences in recognition errors compared to the other three types of partial discharge. Compared to the other three fusion methods, LDA data fusion more effectively eliminates redundant data and achieves complementarity between the two image features. Although the dimensionality reduction effect of KPCA is superior to PCA, it remains less effective than LDA.

5. Conclusions

This paper proposes a new method for partial discharge recognition to address the low accuracy in GIS partial discharge identification. First, the image features of PRPS are extracted, followed by feature selection and fusion. Finally, the fused features are input into an improved recognition model to classify partial discharge types. The main conclusions are as follows: (1) The recognition performance of fused features is superior to the individual CLBP-M and CLBP-S features. (2) Combining feature selection with data dimensionality reduction eliminates redundant information, reduces feature dimensionality, improves model training efficiency, and enhances recognition accuracy. (3) Introducing differential evolution to enhance the BES algorithm has improved the optimization algorithm's search performance. Compared to the BES-SVM, ABC-SVM, and DO-SVM models, the IBES-SVM model achieves higher recognition accuracy.

Use of AI tools declaration

The authors declare they have not used Artificial Intelligence (AI) tools in the creation of this article.

Acknowledgments

This research was funded by State Grid Jiangsu Electric Power Co., Ltd. Technology Project: Research on Improving the Validity of GIS Equipment Partial Discharge Signal Calibration and Monitoring, grant number J2023027.

Conflict of interest

The authors declare no conflicts of interest.

Author contributions

Conceptualization, H.X.; methodology, Z.X.; software, Z.X.; validation, C.Y.; formal analysis, C.Y.; resources, S.C.; writing—original draft preparation, Y.C.

References

1. Tuyet-Doan VN, Pho HA, Lee B, et al. (2021) Deep ensemble model for unknown partial discharge diagnosis in gas-insulated switchgears using convolutional neural networks. *IEEE Access* 9: 80524–80534. https://doi.org/10.1109/ACCESS.2021.3084950
2. Tuyet-Doan VN, Nguyen TT, Nguyen MT, et al. (2020). Self-attention network for partial-discharge diagnosis in gas-insulated switchgear. *Energies*, 13. https://doi.org/10.3390/en13082102
3. Sabot SrA, Petit A, Taillebois JP (1996) GIS insulation coordination: On-site tests and dielectric diagnostic techniques, a utility point of view. *IEEE Trans Power Delivery* 11: 1309–1316. https://doi.org/10.1109/61.517485
4. Li X, Tang H, Mu S, et al. (2012) Partial discharge monitoring system for PD characteristics of typical defects in GIS using UHF method. *2012 International Conference on High Voltage Engineering and Application,* Shanghai, 625–628. https://doi.org/10.1109/ICHVE.2012.6357053

5. Han X, Zhang X, Guo R, et al. (2022) Partial discharge detection in gas-insulated switchgears using sensors integrated with uhf and optical sensing methods. *IEEE Trans Dielectr Electr Insul* 29: 2026–2033. https://doi.org/10.1109/TDEI.2022.3198715
6. Yao R, Li J, Hui M, et al. (2022) Pattern recognition for partial discharge using adaptive boost classification model based on ensemble method. *Power Syst Technol* 46: 2410–2419. https://doi.org/10.13335/j.1000-3673.pst.2021.0780
7. Tang Z, Tang M, Li J, et al. (2018) Discussion on the resemblance of different partial discharges and accuracy of PD pattern recognition of GIS equipment. *High Voltage Eng* 44: 2479–2485. https://doi.org/10.13336/j.1003-6520.hve.20180228001
8. Gao J, Zhang Y, Li X, et al. (2022) Quantitative detection of multicomponent SF6 decomposition products based on Fourier transform infrared spectroscopy combined with CARS-ELM algorithm. *IEEE Trans Instrum Meas*, 71. https://doi.org/10.1109/TIM.2022.3194933
9. Zhang Q, Song H, Jiang Y, et al. (2018) Partial discharge pattern recognition of transformer based on OS-ELM. *High Voltage Eng* 44: 1122–1130. https://doi.org/10.13336/j.1003-6520.hve.20180329011
10. Hu W, Li J, Liu X, et al. (2024) Partial discharge fault identification method for GIS equipment based on improved deep learning. *J Eng*, 2024. https://doi.org/10.1049/tje2.12386
11. Zheng J, Chen Z, Wang Q, et al. (2022) GIS partial discharge pattern recognition based on time-frequency features and improved convolutional neural network. *Energies*, 15. https://doi.org/10.3390/en15197372
12. Wang H, Song S, Qian Y, et al. (2021) Recognition algorithm of GIS partial discharge phase resolved pulse sequence based on CLAHE enhancement. *High Voltage Eng* 47: 3836–3844. https://doi.org/10.13336/j.1003-6520.hve.20201240
13. Wang YX, Yan J, Yang Z, et al. (2023) A novel hybrid *meta*-learning for few-shot gas-insulated switchgear insulation defect diagnosis. *Expert Syst Appl* 233: 120956. https://doi.org/10.1016/j.eswa.2023.120956
14. Li Z, Wang H, Qian Y, et al. (2022) Pattern recognition of partial discharge in the presence of noise based on speeded up robust features. *Trans China Electrotech Soc* 37: 775–785. https://doi.org/10.19595/j.cnki.1000-6753.tces.210018
15. Li Z, Qian Y, Wang H, et al. (2022) Partial discharge fault diagnosis based on zernike moment and improved bacterial foraging optimization algorithm. *Electric Power Syst Res*, 207: 107854. https://doi.org/10.1016/j.epsr.2022.107854
16. Park JY, Oh SK (2021) A Comparative study on CNN-based pattern classifier through partial discharge data processing methods. *Trans Korean Institute Electr Eng* 70: 515–525. https://doi.org/10.5370/KIEE.2021.70.3.515
17. Song S, Qian Y, Wang H, et al. (2020) Partial discharge pattern recognition based on 3D graphs of phase resolved pulse sequence. *Energies*, 13. https://doi.org/10.3390/en13164103
18. Song H, Dai J, Sheng G, et al. (2018) GIS partial discharge pattern recognition via deep convolutional neural network under complex data source. *IEEE Trans Dielectr Electr Insul* 25: 678–685. https://doi.org/10.1109/TDEI.2018.006930
19. Qiang Z, Jianhua A, Xiaoya S, et al. (2022) Extended complete local binary pattern for texture classification. *Multimedia Tools Appl* 81: 5389–5405. https://doi.org/10.1007/s11042-021-11776-1

20. Wang Y, Yan J, Yang Z, et al. (2023) Novel metric-based meta-learning model for few-shot diagnosis of partial discharge in a gas-insulated switchgear. *ISA Trans* 134: 268–277. https://doi.org/10.1016/j.isatra.2022.08.009
21. Wang Y, Yan J, Yang Z, et al. (2023) Simultaneous partial discharge diagnosis and localization in gas-insulated switchgear via a dual-task learning network. *IEEE Trans Power Delivery* 38: 4358–4370. https://doi.org/10.1109/TPWRD.2023.3312704
22. Alpaslan N (2022) Neutrosophic set based local binary pattern for texture classification. *Expert Syst Appl* 209: 118350. https://doi.org/10.1016/j.eswa.2022.118350
23. Liu Q, Chen C, Zhang Y, et al. (2011) Feature selection for support vector machines with RBF kernel. *Artificial Intell Rev* 36: 99–115. https://doi.org/10.1007/s10462-011-9205-2
24. Zhou M, Bian K, Hu F, et al. (2020) A new method based on CEEMD combined with iterative feature reduction for aided diagnosis of epileptic EEG. *Front Bioeng Biotechnol*, 8. https://doi.org/10.3389/fbioe.2020.00669
25. Sholik M, Fatichah C, Amaliah B (2023) Classification of cervical cell images into healthy or cancer using convolution neural network and linear discriminant analysis. *2023 IEEE International Conference on Industry 4.0, Artificial Intelligence, and Communications Technology (IAICT)*, BALI, Indonesia, 383–389. https://doi.org/10.1109/IAICT59002.2023.10205826
26. Alsattar HA, Zaidan AA, Zaidan BB (2020) Novel meta-heuristic bald eagle search optimisation algorithm. *Artificial Intell Rev* 53: 2237–2264. https://doi.org/10.1007/s10462-019-09732-5

AIMS Press